PROCEEDINGS, 50th Workshop on Geothermal Reservoir Engineering
Stanford University, Stanford, California, February 10-12, 2025
SGP-TR-229

Simulating matrix thermal contraction and stochastic fracture networks in enhanced geothermal systems using PFLOTRAN

Hannah S. Gatz-Miller, Jennifer M. Frederick and Thomas S. Lowry

Sandia National Laboratories, 1515 Eubank Ave. SE, Albuquerque, NM 87185

hsgatzm@sandia.gov

Keywords: EGS, numerical modelling, fractures

ABSTRACT

Enhanced Geothermal Systems (EGS) make use of natural and developed fracture connectivity in otherwise low permeability rock to circulate fluid in the subsurface for geothermal power production. Previous work has suggested that the degree of fracture connectivity as well as fracture geometry, can play an outsized role in thermal drawdown and the lifespan of the geothermal plant. Contraction of the rock matrix as cool water is circulated can affect the width of the fracture aperture and therefore the connectivity of the fracture network. Thermo-hydro-mechanical (THM) models are a useful tool to explore these processes. However, fracture networks, as occur in nature, are complex and difficult to model, and thus fracture networks in THM models are often simplified and/or represented as one of many statistically potential interpretations. Whether these statistically derived fracture networks are representative of the subsurface, and how this can impact analysis and understanding of these systems, is a matter of interest.

PFLOTRAN is a parallelized multiphase reactive transport code that is used to simulate subsurface flow and transport, including geothermal processes and fracture flow. A PFLOTRAN fracture process model has been further developed to generate fracture families, defined by key variables describing their orientation, spatial extent, and aperture width, with multiple fractures fulfilling these descriptions that are produced stochastically using a standard deviation from the defined key variables and a random seed number.

An initial 2-D modelled enhanced geothermal system (EGS) simulation featuring a complex background fracture network (100 fractures) separating two wells was constructed and run to demonstrate the potential for preferential flow channeling when thermo-mechanical processes are considered in the model. Five sets of stochastically generated fracture families connecting between injection and production wells were subsequently modelled in a domain with negligible natural background fracture network and low permeability. The random seed numbers defining final fracture location and orientation were varied in six simulations, along with thermally driven changes to fracture aperture (THM). Six counterpart simulations were then run without the thermal changes (TH). Changes in thermal drawdown at the production well between TH and THM simulations, as well as between the different fracture networks, were examined to explore how variation in fracture network extent and fracture orientation may affect these processes and how this may influence our understanding of subsurface fracture flow in the context of EGS.

1. INTRODUCTION

Fracture connectivity between injection and production wells in enhanced geothermal systems (EGS) can be produced by hydraulic stimulation (e.g. fracking) of naturally low permeability rock at depth until connectivity between injection and production wells is achieved (Li et al., 2022; Olasolo et al., 2016). Generating fractures that fully connect and allow for significant fluid flow between wells at depth is an impressive engineering problem and, while the eventual creation and existence of connectivity can be established via a variety of tools, including well tests and subsurface imaging, the exact orientation, geometry, and type of connectivity between fractures may be difficult as well as expensive to assess (e.g. Fu et al., 2021). Previous work (Liu et al., 2022; Fu et al., 2016; Gringarten et al., 1975) suggests that increased proportion of fracture-matrix surface area as well as (with quantity depending on the system) distance between fractures connecting the wells, can lead to more and prolonged heat extraction and increased lifespan of the geothermal plant. Therefore, it is very useful to understand the orientation and location of the fractures connecting injection and production wells (Liu et al., 2022).

From a modeling perspective, uncertainty regarding fracture orientation and location has been dealt with by defining a number of fracture variables, including fracture shape, orientation and extent, and then generating a series of statistically probable fractures and fracture families in the modeled subsurface to explore trends and processes (Fu et al., 2016; Lei et al., 2017). This methodology has the benefit of exploring a range of potential fracture placements but, if the need is to simulate a particular system, such models can be limited by the uncertainty inherent in not knowing which statistically generated variation is closest to reality. It is therefore of interest to explore the extent to which differences in stochastically generated fractures in the context of EGS may affect rates of thermal drawdown and geothermal power production, compared to other processes such as changes in fracture aperture due to cooling, and potential development of preferential flow pathways (Liao et al., 2023; Liu et al., 2022). Previous work (e.g. Fu et al. 2016) have explored this concept with discretely simulated stochastic fracture networks, and determined a significant difference in

thermal drawdown between different networks with the same statistical characteristics, as well as with and without inclusion of mechanical processes. Previous work suggests a trend wherein inclusion of mechanical processes when modeling pumping within an expansive fracture network, can result in preferential flow channeling of cool water and a steeper drawdown curve versus simulations without mechanical processes. Given the popularity and increasing use of reactive transport models, which utilize Equivalent Continuum Porous Medium (ECPM) domains and are used to simulate EGS with varying degrees of complexity, it is useful to understand and compare the behavior of models that will be used to combine reactive transport and fracture flow in an ECPM domain, when simulating stochastic fracture networks as well.

To this end, we first demonstrate previously described preferential flow channeling processes utilizing a stochastically generated complex background fracture network between injection and production wells in a PFLOTRAN ECPM domain. We then model a series of six 2D subsurface EGS simulations meant to be representative of a region with negligible background fractures, where the primary source of connectivity between injection and production wells is due to fracking. For these "fracking only" simulations, stochastically generated fracture families linking injection and production wells are defined by several key variables, and then varied only by changing the random seed number used to generate the vector normal to the fracture plane. This small change in each otherwise identical simulation produces fracture families of slightly different orientation with subsequent varying degrees of connectivity between injection and production wells, to investigate any resulting difference in thermal drawdown between equivalently potential stochastic simulations, and the implications for power production.

2. METHOD

2.1 PFLOTRAN

The simulations were constructed using PFLOTRAN, an open-source reactive transport code that can simulate subsurface flow, transport, and thermal processes in an equivalent continuous porous medium in up to three dimensions (Hammond et al., 2014; Lichtner et al., 2015). Since 2023, PFLOTRAN has been under development to further include fracture modeling capability, including defining and generating single (deterministic) fractures and stochastic fracture families directly in PFLOTRAN, and changing fracture aperture due to thermal changes during the simulation (Frederick et al., 2025). Fracture families in PFLOTRAN are defined by the number of fractures (-), the fracture aperture width normal to the fracture plane (m), the fracture set center (x, y, z coordinates on the domain grid), the fracture radial extent (m), and the orientation of the vector normal to the fracture plane (x, y, z). Each term is further described by an allowed standard deviation from the assigned values, as well as a random seed number used to generate the final fracture extent, orientation, and location within the limits of the standard deviation. As PFLOTRAN represents an Equivalent Continuum Porous Medium (ECPM) domain, fractures are not simulated discretely, but interpret fracture-containing grid cells as a sum of both fracture-space and matrix material, with such cells presenting as zones of higher permeability and porosity versus cells without any fractures. Fracture permeability and cell porosity are calculated as a function of fracture aperture (1, 2, 3). If thermal matrix changes are included, these values are updated in each time step to reflect change in fracture aperture due to contraction of the matrix length normal to the aperture (4).

$$\emptyset^{\boldsymbol{f}} = \emptyset + \alpha \boldsymbol{\mathcal{L}^{-1}} \tag{1}$$

$$K_{xx}^{f} = K_{yy}^{f} = \frac{1}{12}\alpha^{3}\boldsymbol{\mathcal{L}^{-1}} \tag{2}$$

$$K_{zz}^{f} = 0 \tag{3}$$

$$\Delta L = \delta \Delta T \boldsymbol{\mathcal{L}} \tag{4}$$

Where $\emptyset^{\boldsymbol{f}}$ **i**s fractured grid-cell porosity (m^3 m^{-3}), $\emptyset$ is initial porosity (m^3 m^{-3}), and $\alpha/\boldsymbol{\mathcal{L}}$ is fracture aperture over the grid cell length normal to the fracture plane (m m^{-1}). K_{xx}^{f}, K_{yy}^{f}, K_{zz}^{f} are permeability in the orientation of the fracture plane in *x* and *y* direction with *z* normal to the plane (m^2). ΔL is the change in matrix length (m) normal to the fracture plane due to matrix thermal contraction where δ is the thermal expansion coefficient of the matrix material (m m^{-1} $°C^{-1}$), ΔT is the change in temperature (°C). See Gatz-Miller et al. (2024), Frederick et al. (2025) for further detail with respect to equations and implementation of fracture families.

2.2 Model Domain and Boundary Conditions

The flow domain for all simulations (Fig. 1) was 2-dimensional and between -3000.0 m and -2750.0 m depth (z-direction), a lateral distance of 298.0 m (x-direction), and 1.0 m width (y-dimension). Grid cells were 1.0 m x 1.0 m x 1.0 m. All domain boundaries were impermeable except for the production well outlet, which was a 1.0 m^3 outlet on the western boundary (x = 0 m) at a depth of -2800.0 m (Fig. 1). Initial pressure was hydrostatic, calculated for depths of 2750-3000 m below the ground surface and ranged between 26.1 MPa and 28.2 MPa. Initial temperature was calculated assuming 0.06° C per m gradient increase with depth from land surface for an initial temperature range between 165°-178° C. Matrix material was set as low permeability ($1.0 \cdot 10^{-18}$ m^2) granite (Selvadurai et al., 2005), and the thermal expansion coefficient in the THM simulations for granite at approximately 200° C (between $4.0 – 10.0 \cdot 10^{-6}$ m m^{-1} $°C^{-1}$) (Heuze, 1983) was increased by an order of magnitude to compensate for the current

functionality of the fracture process model which considers only the length change of the material in the grid cell with the fracture and not the surrounding material. Thermal conductivity of the matrix material was 1.40 W m^{-1} °C^{-1} when dry and 2.75 W m^{-1} °C^{-1} when wet, and rock density was 2.8 g cm^{-3} with a specific heat of 0.9 J g^{-1} K^{-1} (Heuze, 1983; Miao et al., 2014). For the "fracking only" simulations, higher permeability well material ($1.0 \cdot 10^{-8}$ m^2) for the production well was placed between 0.0 m and 235.0 m lateral extent (x-direction) at - 2800.0 m, and for the injection well between 68.0 m and 298.0 m lateral extent and -2950.0 m.

For the complex fracture network simulation, fifty conjugate fracture families (100 fractures) making up a "natural" background complex fracture network with varying degrees of connectivity, and one "fracked" connecting fracture between injection and production wells, were used for the initial simulation demonstrating flow channeling in PFLOTRAN THM simulations. The connecting fracture was assigned a fracture aperture three times greater than the background fracture network to mimic limited fracture connectivity in a natural network compared to large fractures engineered (fracked) to facilitate connection between injection and production wells in EGS (table 1). This complex fracture network was run with both TH and THM capabilities to demonstrate PFLOTRAN's ability to replicate the flow channeling processes within fracture networks between wells described in previous works (e.g. Fu et al., 2016; Liao et al., 2023).

For the subsequent "fracking only" simulations, reference fracture networks from the Utah FORGE project (Finnila and Jones, 2024) describing discrete fractures and conjugate fracture sets between injection and production wells, were used as a basis for fracture type, general orientation, and location. Each simulation included five fracture families made up of two conjugate fractures (table 1 and 2). The fracture families were oriented in the domain to form some degree of connectivity between the two wells to mimic potential fracked pathways for fluid flow developed for EGS in a subsurface lacking any notable natural background fracture network or connectivity. Six simulations were run by varying the random seed number used to generate the vector normal to the fracture planes, and fracture families were otherwise assigned the same characteristics for all simulations (Table 1). For each simulation (1 through 6), the seed number for only the vector normal to each fracture plane was randomly assigned to generate variation within fractures that were otherwise identically defined. The six simulations were run with the matrix thermal contraction capability activated (THM simulations), and then rerun without activation (TH simulations).

Initial permeabilities for the fracture zones for all simulations were calculated internally by PFLOTRAN (equations 1-4) and were on the order of $1.0 \cdot 10^{-9}$ m^2 to $1.0 \cdot 10^{-8}$ m^2. Injection rate at the injection well was $3 \cdot 10^{-2}$ kg s^{-1} m^{-2} at a temperature of 60.0°C, calibrated to account for model dimensionality and for reasonable rates of thermal drawdown over the course of forty years in a similarly sized system based on the literature (e.g. Olasolo et al. 2016; White et al. 2018; Yan et al. 2018).

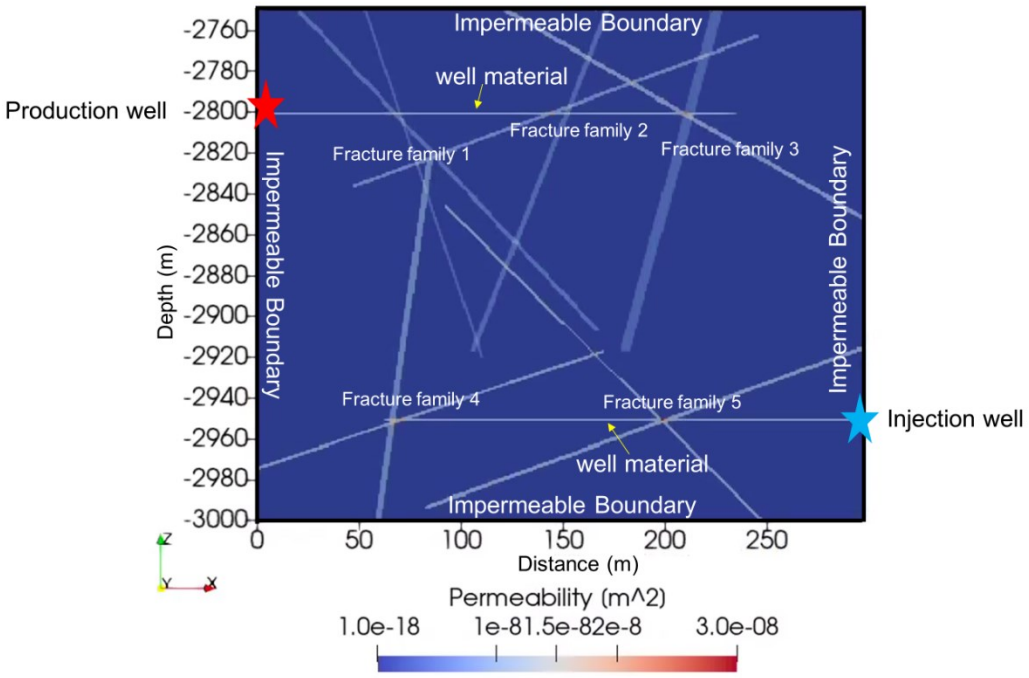

Figure 1: Model domain and example of "fracking only" fracture network with five fracture families.

Table 1: Fracture Characteristics

Fracture Characteristic	Complex Network	Connecting	Fracked Only
Number of fractures in family	2	n/a	2
Fracture aperture assigned value	$5.0 \cdot 10^{-3}$ m	$1.5 \cdot 10^{-2}$ m	$5.0 \cdot 10^{-3}$ m
Fracture aperture allowed standard deviation	$3.0 \cdot 10^{-2}$ m	n/a	$3.0 \cdot 10^{-4}$ m
Fracture aperture allowed maximum	$1.0 \cdot 10^{-2}$ m	n/a	$1.0 \cdot 10^{-2}$ m
Standard deviation for x-coordinate from assigned fracture set center	2.0 m	n/a	2.0 m
Standard deviation for y-coordinate from assigned fracture set center	0.5 m	n/a	0.5 m
Standard deviation for z-coordinate from assigned fracture set center	2.0 m	n/a	2.0 m
Standard deviation for assigned normal vector x-coordinate	0.5 m	n/a	0.5 m
Standard deviation for assigned normal vector y-coordinate	0.5 m	n/a	0.5 m
Standard deviation for assigned normal vector z-coordinate	0.5 m	n/a	0.5 m
Fracture radius (extent from center) in x -direction	25.0 m	140.0 m	100.0 m
Fracture radius (extent from center) in y -direction	1.5 m	1.5 m	1.5 m
Fracture radius (extent from center) in z -direction	25.0 m	140.0 m	120.0 m
Standard deviation for assigned radius x-direction	10.0 m	n/a	10.0 m
Standard deviation for assigned radius y-direction	0.5 m	n/a	0.5 m
Standard deviation for assigned radius z-direction	10.0 m	n/a	10.0 m

Table 1 describes characteristics for the stochastically generated fracture families in the complex fracture network, the single fracture connecting injection and production wells emplaced within the complex network, and the simple network for the subsequent simulations representing a subsurface with negligible natural fractures and fractures present due to fracking only.

Table 2: Fracture Family Placement

Fracture Family	Fracture Center Coordinates (x, y, z)	Well	Normal Vector Coordinates (x, y, z)
1	(70.0, 0.5, -2800.0)	Production	(0.5, 0.0, 0.5)
2	(150.0, 0.5, -2800.0)	Production	(0.5, 0.0, 0.5)
3	(210.0, 0.0, -2800.0)	Production	(0.25, 0.0, -0.5)
4	(70.0, 0.5, -2950.0)	Injection	(0.5, 0.0, -0.5)
5	(200.0, 0.5, -2950.0)	Injection	(0.5, 0.0, 0.5)

Table 2 describes fracture placement for the five fracture families in the "fracking only" simulations. Adjusting only the random seed number defining the vector normal to the fracture plane generated six different simulations.

3. RESULTS

3.1 Complex fracture network

Permeability increased in all fractures of the complex fracture network, with the greatest increase in the fractures with the most flow, and particularly in the direct connection between injection and production wells (Fig. 2). Initial permeability for fractures in the fracture network increased from 7.0 to $9.0 \cdot 10^{-9}$ m^2 to $1.0 \cdot 10^{-8}$ m^2 to $5.0 \cdot 10^{-8}$ m^2 after forty years, while the connecting fracture increased permeability from initial permeability of $2.8 \cdot 10^{-8}$ m^2, to an order of $4.0 \cdot 10^{-7}$ m^2 near the production well and $6.2 \cdot 10^{-7}$ m^2 near the injection well after forty years (Fig. 2). Thermal drawdown at the production well was greater in the THM simulation by up to 4°C compared to the TH simulation, particularly during the middle and latter half of the simulation (between 15-30 years) (Fig. 3). Fluid in the TH simulation expanded more into the background fracture network, while in the THM simulation, cold water tended to move through the most permeable direct connecting fracture, further cooling them and increasing permeability, demonstrating the potential for flow channeling and a steeper thermal drawdown curve when thermo-mechanical processes are considered in fracture flow modeling (Fig. 3).

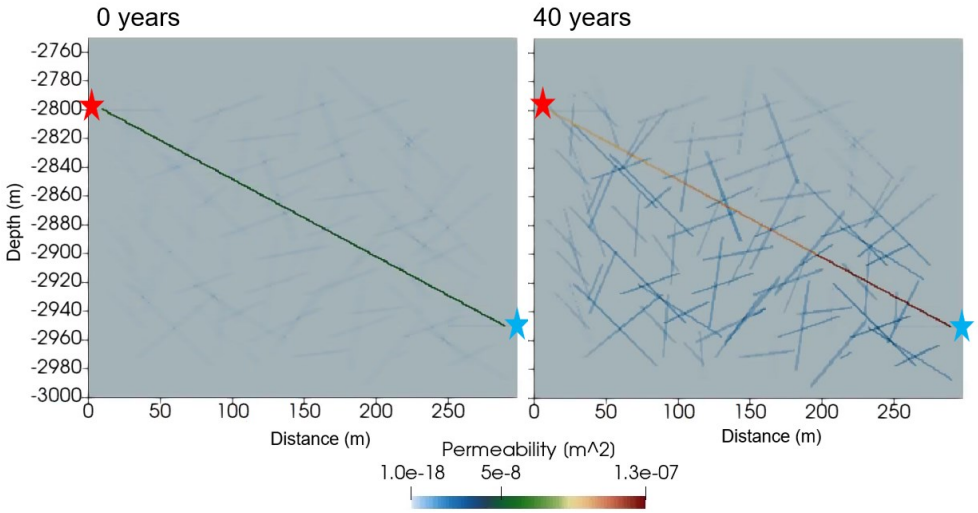

Figure 2: Complex fracture network in THM simulation with permeability after 40 years. The blue and red stars indicate the injection and production well locations respectively.

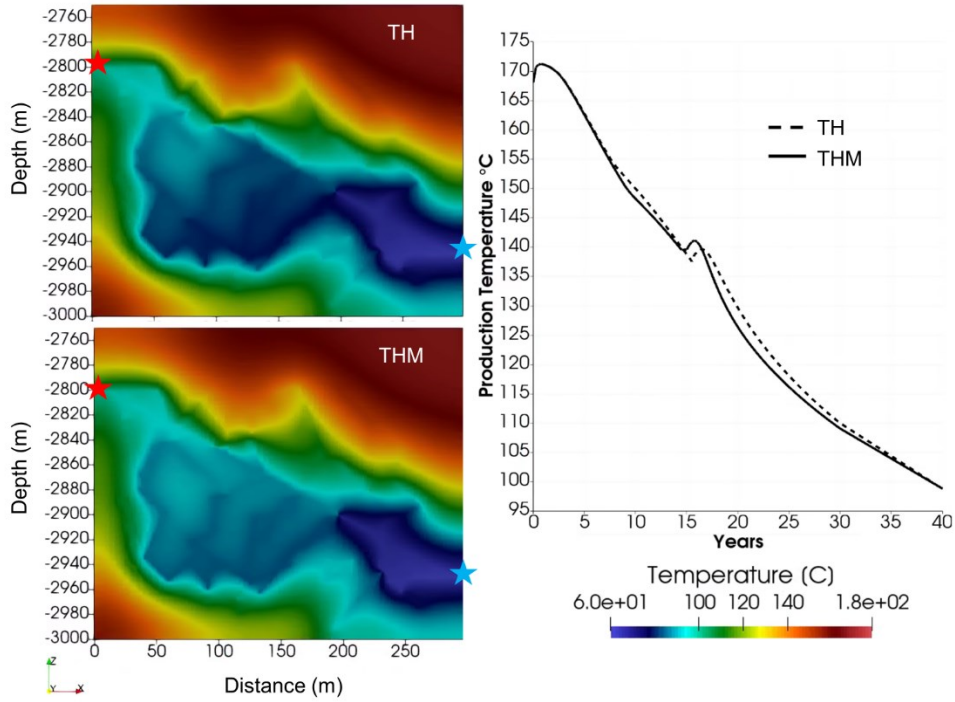

Figure 3: Complex fracture network in TH and THM simulation showing temperature and thermal drawdown after 40 years. The blue and red stars indicate the injection and production well locations respectively.

3.2 "Fracking only" network

Six simulations generated five sets of fracture families, each with slightly different orientations and differing degrees of connectivity between injection and production wells (Fig. 4). For the THM simulations, the range of maximum permeability in the fracture zones increased from a range of $1.0 \cdot 10^{-9}$ m^2 - $1.0 \cdot 10^{-8}$ m^2 (with some permeability at fracture intersections on the order of $3.0 \cdot 10^{-8}$ m^2) to a range of $1.0 \cdot 10^{-8}$ m^2 - $5.0 \cdot 10^{-8}$ m^2, depending on location and the flow pattern of the injected water (Fig. 5). The difference in fracture connectivity and location generated a notable difference in thermal drawdown at the production well over the course of forty years, with five of the simulations showing a final temperature at the production well output ranging between 98° C and 104° C, and the hottest outlier finishing at 111° C (Fig. 6). TH simulations (i.e. without thermal matrix

contraction) differed slightly from their THM counterparts in the whole of the domain (Fig. 7), but only up to 1.0 ° C at the production well (Fig. 6 and 7). Further, while there were preferential flow paths depending on the fracture orientation and connectivity, they did not appear to vary between THM and TH simulation counterparts and, where there was difference between TH and THM simulations, TH simulations were cooler than their THM counterparts (Fig. 7 and 8).

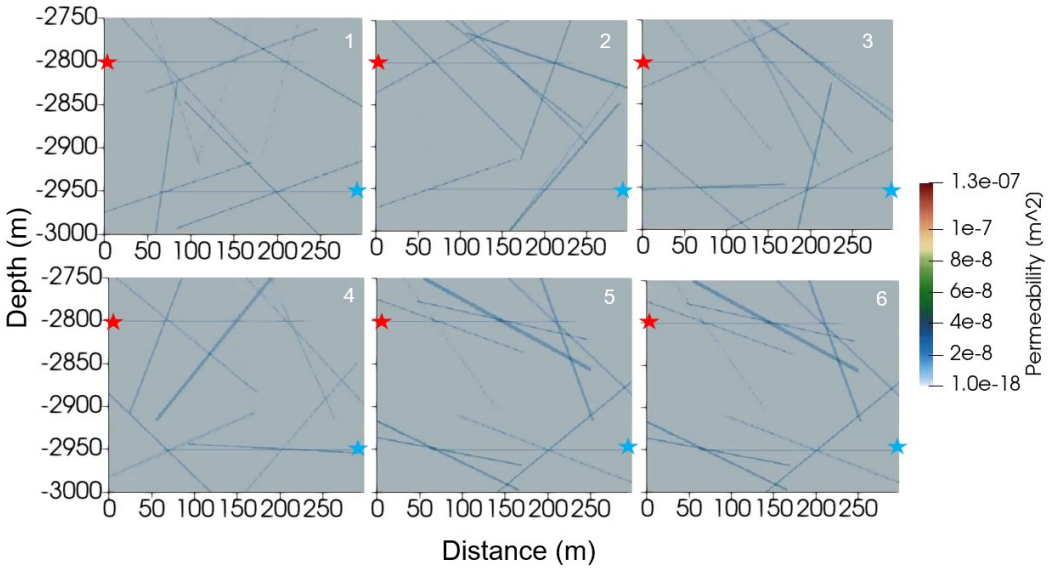

Figure 4: Initial permeability for both TH and THM "fracking only" simulations 1-6. Blue and red stars are placed at the injection and pumping wells respectively.

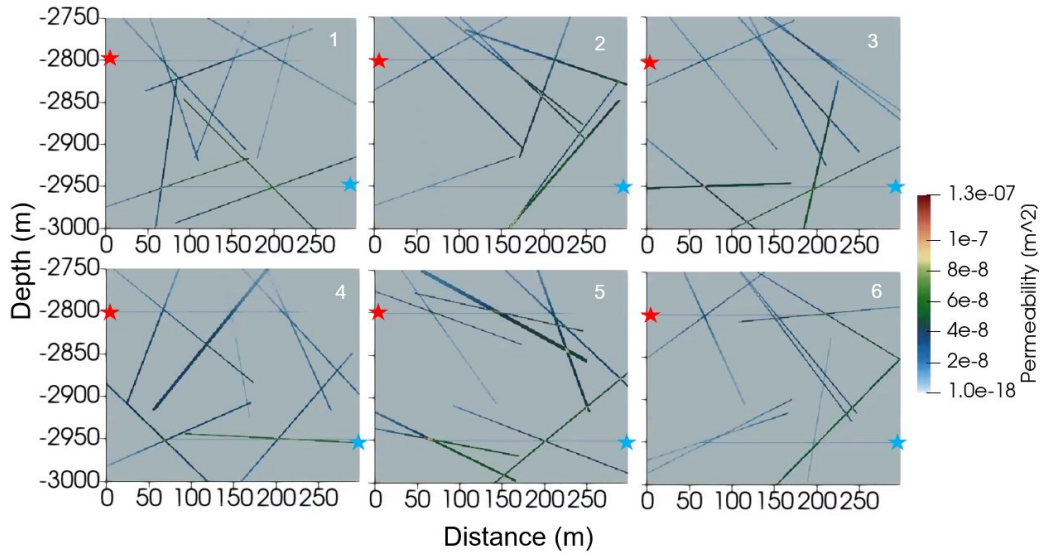

Figure 5: Fracture permeability after forty years in THM simulations 1-6. Blue and red stars are placed at the injection and pumping wells respectively.

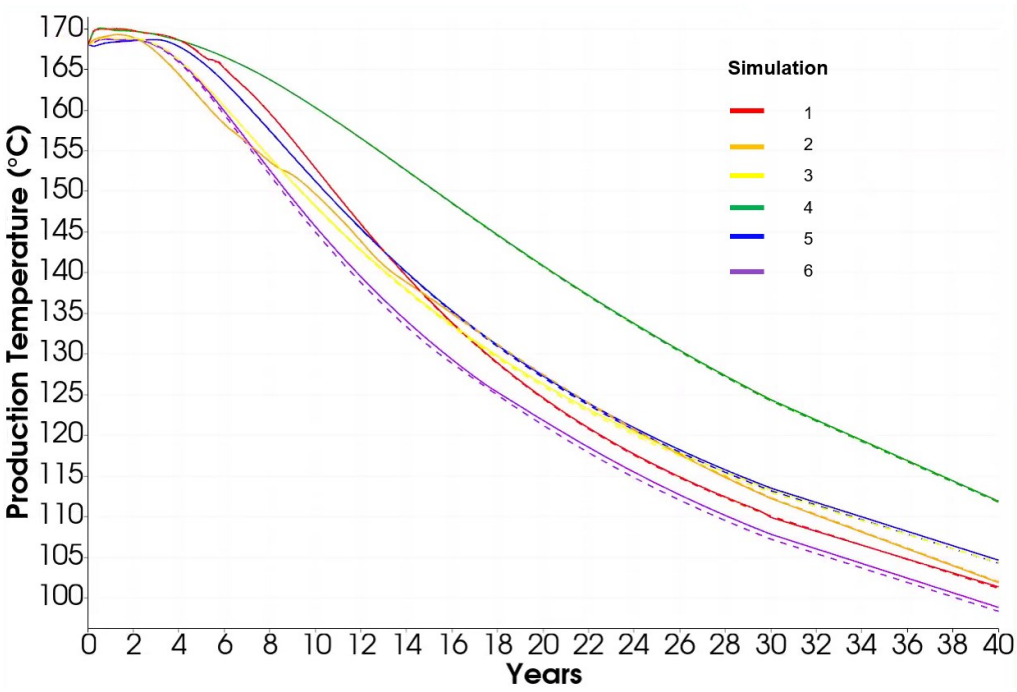

Figure 6: Temperature at the production well over the course of forty years. Solid lines represent THM simulations, dashed lines of the same color represent counterpart TH simulations.

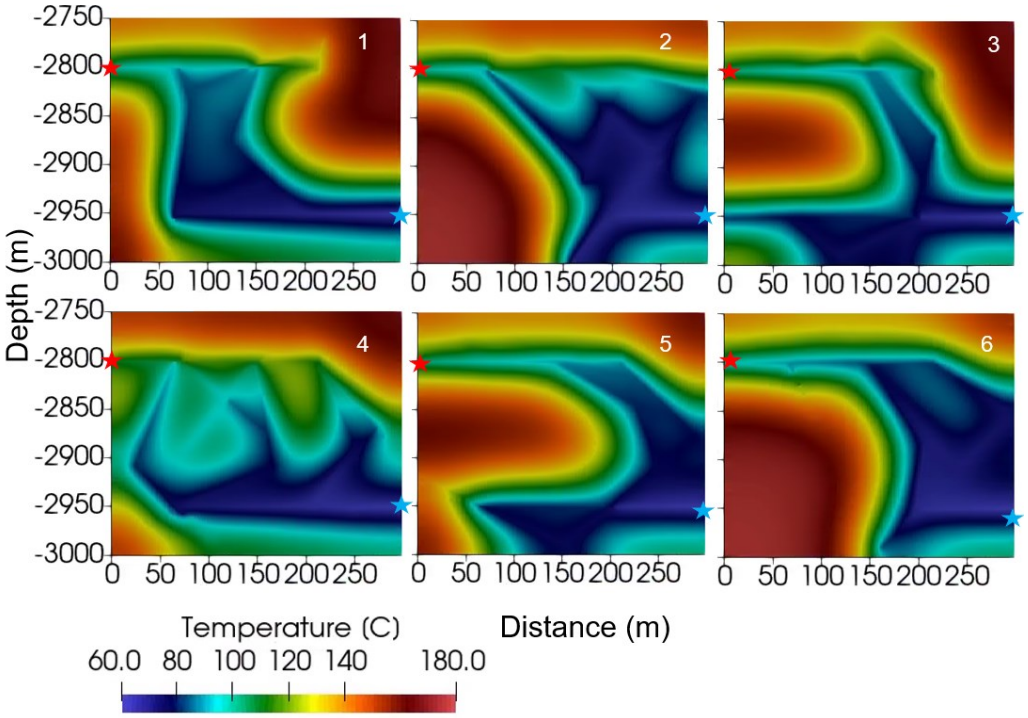

Figure 7: Temperature in THM simulations 1-6 after 40 years. Blue and red stars are placed at the injection and pumping well respectively.

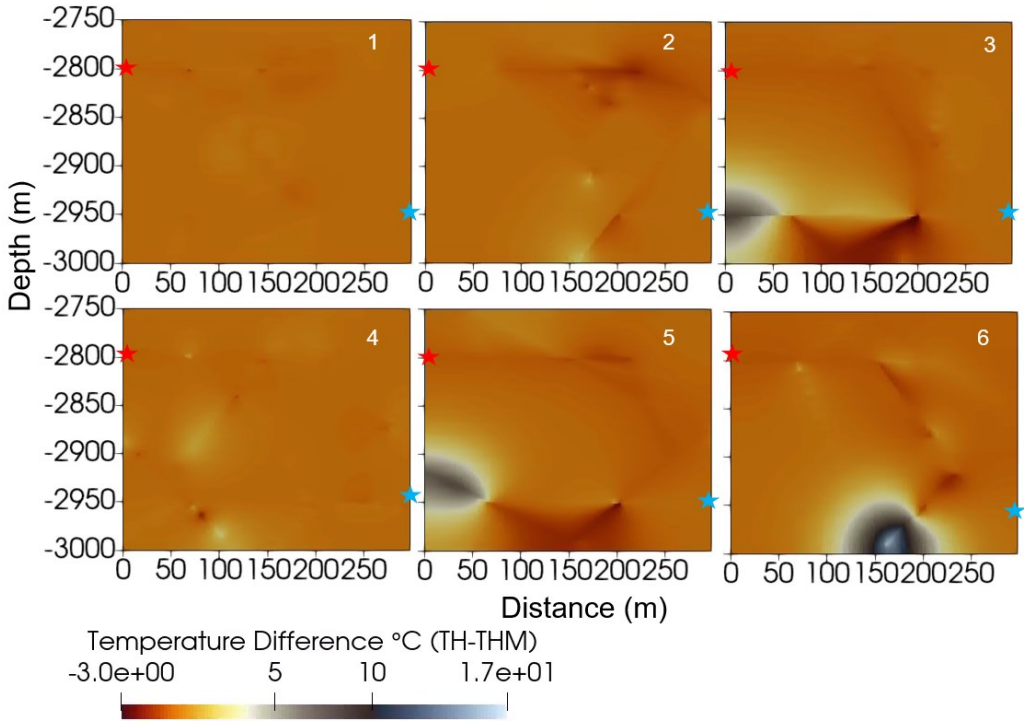

Figure 8: Temperature difference mapped between TH and THM simulations 40 years. Blue and red stars are placed at the injection and pumping well respectively. Though there were differences of up to 17°C between TH and THM in the whole domain, temperature differences were limited at the pumping well.

4. DISCUSSION

Stochastic generation of fracture networks to compensate for limited data regarding subsurface conditions is a useful technique that returns a range of potential outcomes for fluid flowpath and heat extraction. The initial simulation with the complex background fracture network demonstrates the previously described (e.g. Fu et al., 2016; Liao et al., 2023) flow channeling when thermo-mechanical processes are taken into account. Cool water causes matrix material to contract, increasing fracture aperture such that even more cool water may flow through the widened fracture aperture, further increasing it in a positive feedback loop, and flow then channels mainly through the most connected fractures. The result of this preferential flow channeling is a steeper thermal drawdown curve at the production well compared to a simulation that does not take these processes into account. For TH simulations, the main flow channels are less distinct and cannot widen further, so fluid is instead more likely to move into the wider background fracture network. With more and expanded surface area from which heat may be extracted, the thermal drawdown curve for the TH simulation is shallower compared to the THM. We do find there was some difference in the slope of the TH drawdown curve shown in this work (steeper) compared to previous work (shallower) (Fu et al., 2016). We suggest that this may be due to the much smaller domain and fracture network used in this work, and wells that are closer together (only 150 m rather than 400 to 800 m). Additionally, the current code for thermal contraction (see equation 4) is only implemented in the fracture-containing grid cell and not the neighboring cells which might limit mechanical thermal changes. Though thermal expansion coefficient was already somewhat calibrated for this work, it or the process model itself may need to be further adjusted.

Results from the “fracking only” simulations showed only a slight difference in thermal drawdown between the THM versus TH simulations and, where there was any difference between them, the THM simulations were slightly hotter at the production well—the opposite of the trend observed in the “complex fracture network” simulation. Mapping flow and temperature of these simulations suggests that the lack of background fracture networks in the “fracking only” simulations compared to the previous simulation limits availability for any alternative flow pathways for both TH and THM and so the main flow routes for TH and THM are essentially identical. Meanwhile, dead-end fractures did widen in THM simulations, allowing for some additional fluid-surface area connection, while this process was less notable in the TH simulation, resulting in THM simulations that were consistently slightly hotter at the production well versus counterpart TH simulations.

In contrast to TH vs THM, even a small variation in how the fracture families were oriented and thus connected, resulted in up to a 20° C difference in potential thermal output—a variation that would likely have significant implications for power generation. Fracture networks that covered a wider area and were more connected (e.g., simulations #4 and #5), were able to retain more heat from the surrounding rock versus those with limited connectivity (e.g., simulations #1 and #6). These results are in agreement with

previous work indicating the importance of fracture-matrix surface area and fracture distance to maximizing heat renewal over a longer period of time (e.g., Gringarten et al. 1975; Liu et al. 2022).

The simulations shown here are limited in domain and scope and use a modelling capability still under development. Considered together, results from all simulations suggest interesting trends with regards to modeling fracture systems and EGS. The "complex fracture network" simulation suggests that if such a network is present in the subsurface, then flow channeling will likely take place if mechanical processes are considered. As the thermal drawdown difference between TH and THM simulations may be enough to affect power production, it may be useful to consider mechanical processes in the modeling to avoid over-estimating reservoir heat availability. However, if there is no or extremely limited background fracture network and the only link between wells is a few fractures engineered specifically to facilitate connectivity, then there may be negligible difference in thermal drawdown between TH and THM simulations and no real need to include THM in the modeling when TH alone will suffice. Instead, efforts to map fracture location and connection may be more useful as these six simulations where only a random seed number defining fracture orientation was varied, have demonstrated a significant difference in flow and thermal drawdown when there are few fractures and fracture connection is limited.

5. CONCLUSION

These preliminary results suggest that random fracture orientation has the potential to significantly affect rates of thermal drawdown versus inclusion of mechanical processes, if modelling EGS under the conditions of a limited natural background fracture network. While stochastically generated fracture networks are a useful tool for simulating subsurface fracture flow in EGS, small variation in even simple networks can significantly affect connectivity and lead to tens of degrees difference in thermal drawdown over the lifetime of a geothermal power plant. In comparison, a simulation with an extensive and complex fracture network may require additional mechanical processes (THM) in the modeling to account for flow channeling. Further work is needed to identify exactly which fracture network characteristics require THM modeling versus those that may not. If modeling a particular system, effort should be made to map existing fracture networks and potential fluid flowpaths, as this will allow for model parameterization closest to reality. If stochastically generated fractures are used to model these systems, care should be taken to discuss results as a range, given the limits of the modelling. Further exploration into network extent and complexity, and the amount of subsequent model complexity needed to reasonably capture the subsurface, will improve understanding of how such systems behave, best courses to follow when modelling, and implications for geothermal power production.

ACKNOWLEDGEMENTS

The work presented in this paper was funded by the U.S. Department of Energy, Geothermal Technologies Office.

This paper describes objective technical results and analysis. Any subjective views or opinions that might be expressed in the paper do not necessarily represent the views of the U.S. Department of Energy or the United States Government.

Sandia National Laboratories is a multimission laboratory operated by National Technology and Engineering Solutions of Sandia LLC, a wholly owned subsidiary of Honeywell International Inc., for the U.S. Department of Energy's National Nuclear Security Administration.

SAND2025-01231C.

REFERENCES

Finnila, A., Jones, C., 2024. Updated Reference Discrete Fracture Network Model at Utah FORGE, in: 49th Workshop on Geothermal Reservoir Engineering, SGP-TR-227. Stanford University, California.

Frederick, J.M., Gatz-Miller, H., Lowry, T.S., 2025. Introducing PFLOTRAN's New Geothermal Fracture Model for Simulation of Geothermal Systems, in: PROCEEDINGS, 50th Workshop on Geothermal Reservoir Engineering. Presented at the Stanford Geothermal Workshop.

Fu, P., Hao, Y., Walsh, S.D.C., Carrigan, C.R., 2016. Thermal Drawdown-Induced Flow Channeling in Fractured Geothermal Reservoirs. Rock Mechanics and Rock Engineering 49, 1001–1024. https://doi.org/10.1007/s00603-015-0776-0

Fu, P., Schoenball, M., Ajo-Franklin, J.B., Chai, C., Maceira, M., Morris, J.P., Wu, H., Knox, H., Schwering, P.C., White, M.D., Burghardt, J.A., Strickland, C.E., Johnson, T.C., Vermeul, V.R., Sprinkle, P., Roberts, B., Ulrich, C., Guglielmi, Y., Cook, P.J., Dobson, P.F., Wood, T., Frash, L.P., Huang, L., Ingraham, M.D., Pope, J.S., Smith, M.M., Neupane, G., Doe, T.W., Roggenthen, W.M., Horne, R., Singh, A., Zoback, M.D., Wang, H., Condon, K., Ghassemi, A., Chen, H., McClure, M.W., Vandine, G., Blankenship, D., Kneafsey, T.J., 2021. Close Observation of Hydraulic Fracturing at EGS Collab Experiment 1: Fracture Trajectory, Microseismic Interpretations, and the Role of Natural Fractures. Journal of Geophysical Research: Solid Earth 126, e2020JB020840. https://doi.org/10.1029/2020JB020840

Gatz-Miller, H., Frederick, J.M., Lowry, T.S., 2024. The Combined Effect of Mineral Dissolution/Precipitation and Matrix thermal Contraction on Fracture Aperture in Enhanced Geothermal Systems: A Reactive Transport Approach, in: PROCEEDINGS, 49th Workshop on Geothermal Reservoir Engineering. Presented at the Stanford Geothermal Workshop.

Gringarten, A.C., Witherspoon, P.A., Ohnishi, Y., 1975. Theory of heat extraction from fractured hot dry rock. Journal of Geophysical Research (1896-1977) 80, 1120–1124. https://doi.org/10.1029/JB080i008p01120

Hammond, G.E., Lichtner, P.C., Mills, R.T., 2014. Evaluating the performance of parallel subsurface simulators: An illustrative example with PFLOTRAN. Water Resources Research 50, 208–228. https://doi.org/10.1002/2012WR013483

Heuze, F.E., 1983. High-temperature mechanical, physical and Thermal properties of granitic rocks—A review. International Journal of Rock Mechanics and Mining Sciences & Geomechanics Abstracts 20, 3–10. https://doi.org/10.1016/0148-9062(83)91609-1

Lei, Q., Latham, J.-P., Tsang, C.-F., 2017. The use of discrete fracture networks for modelling coupled geomechanical and hydrological behaviour of fractured rocks. Computers and Geotechnics 85, 151–176. https://doi.org/10.1016/j.compgeo.2016.12.024

Li, S., Wang, S., Tang, H., 2022. Stimulation mechanism and design of enhanced geothermal systems: A comprehensive review. Renewable and Sustainable Energy Reviews 155, 111914. https://doi.org/10.1016/j.rser.2021.111914

Liao, J., Xu, B., Mehmood, F., Hu, K., Wang, H., Hou, Z., Xie, Y., 2023. Numerical study of the long-term performance of EGS based on discrete fracture network with consideration of fracture deformation. Renewable Energy 216, 119045. https://doi.org/10.1016/j.renene.2023.119045

Lichtner, P., Hammond, G.E., Lu, C., Karra, S., Bisht, G., Benajmin, A., Mills, R., Jitendra, K., 2015. PFLOTRAN User Manual: A Massively Parallel Reactive Flow and Transport Model for Describing Surface and Subsurface Processes.

Liu, J., Xue, Y., Zhang, Q., Wang, H., Wang, S., 2022. Coupled thermo-hydro-mechanical modelling for geothermal doublet system with 3D fractal fracture. Applied Thermal Engineering 200, 117716. https://doi.org/10.1016/j.applthermaleng.2021.117716

Miao, S.Q., Li, H.P., Chen, G., 2014. Temperature dependence of thermal diffusivity, specific heat capacity, and thermal conductivity for several types of rocks. Journal of Thermal Analysis and Calorimetry 115, 1057–1063. https://doi.org/10.1007/s10973-013-3427-2

Olasolo, P., Juarez, M.C., Morales, M.P., D'Amico, S., Liarte, I.A., 2016. Enhanced geothermal systems (EGS): A review. Renewable and Sustainable Energy Reviews 56, 133–144. https://doi.org/10.1016/j.rser.2015.11.031

Selvadurai, A.P.S., Boulon, M.J., Nguyen, T.S., 2005. The Permeability of an Intact Granite. pure and applied geophysics 162, 373–407. https://doi.org/10.1007/s00024-004-2606-2

White, M., Fu, P., McClure, M., Danko, G., Elsworth, D., Sonnenthal, E., Kelkar, S., Podgorney, R., 2018. A suite of benchmark and challenge problems for enhanced geothermal systems. Geomechanics and Geophysics for Geo-Energy and Geo-Resources 4, 79–117. https://doi.org/10.1007/s40948-017-0076-0

Yan, X., Liu, Y., Wang, G., Lu, Y., 2018. Optimal injection rate of water in the Guide Basin hot dry rock mining project. Energy Exploration & Exploitation 37, 721–735. https://doi.org/10.1177/0144598718800729